Thermochimica Acta 510 (2010) 82–87

Contents lists available at ScienceDirect

Thermochimica Acta

journal homepage: www.elsevier.com/locate/tca

Thermal analysis during solidification of cast Al–Si alloys

A.A. Canales [a], J. Talamantes-Silva [b], D. Gloria [c], S. Valtierra [c], R. Colás [d,*]

[a] Cuprum, S.A. de C.V., Diego Díaz de Berlanga 95-A, 66480 San Nicolás de los Garza, NL, Mexico
[b] Nemak, S.A. de C.V., Libramiento Arco Vial km 3.8, 66000 García, NL, Mexico
[c] Owens Corning, Privada La Puerta 1110-A, 66350 Santa Catarina, NL, Mexico
[d] Facultad de Ingeniería Mecánica y Eléctrica, Universidad Autónoma de Nuevo León, A.P. 149-F, 66451 San Nicolás de los Garza, NL, Mexico

ARTICLE INFO

Article history:
Received 23 November 2009
Received in revised form 24 June 2010
Accepted 28 June 2010
Available online 7 July 2010

Keywords:
Aluminium
Casting
Solidification
Thermal analysis

ABSTRACT

Solidification of a series of aluminium alloys was studied by means of thermal analysis; the study was centred on the effect that silicon and iron exert on the temperatures for the onset of different microstructural characteristics. The alloys were prepared in a gas fired furnace and were poured into graphite moulds instrumented with a type K thermocouple. The cooling curve was registered with the aid of a computer-driven data logging system and was derived to determine the temperatures for the onset of the formation of pre-eutectic aluminium dendrites, and those for the Al–Si eutectic and for a complex Al–Si–Cu–Mg eutectic. It was found that silicon exerts a strong influence on the two former temperatures, whereas the third one is independent of the content of silicon or iron.

1. Introduction

The demand for the increment in fuel efficiency in automobiles without impairing their performance is one of the driving forces behind the development of newer products and processes in such a competitive industry. Replacement of cast iron by light metals alloys has become commonplace for parts such as cylinder heads, engine blocks and manifolds [1,2]. Aluminium alloys offer the advantage in engine components of enhancing their power rating as the higher thermal conductivity of these alloys, in comparison with cast irons, allow for higher working temperatures in the combustion chamber that contributes in delivering more power per cylinder size while requiring lower amounts of refrigeration liquids [3–5].

Changing from iron to aluminium has not been an easy task for industry, as it is required for aluminium parts to withstand more stringent conditions than those to which iron castings are subjected, which are promoted by the higher working temperatures of the engine that may enhance the reduction in strength of the material at the time that increases the possibility of promoting thermal fatigue [1,6]. Most alloys used in power train applications contain silicon within the hypoeutectic range, and some of them are produced from scrap, as automotive industry exerts a strong policy in reducing costs. The microstructure in the castings would be a mixture of pre-eutectic aluminium dendrites surrounded by the Al–Si eutectic aggregate, but the presences of tramp elements from the scrap promote the formation of intermetallic phases. Iron is always present in scrap and contributes to form at least two phases which are Al_5FeSi and $Al_{15}(Mn,Fe)_3Si_2$, the former being the most dangerous as it is brittle and occurs in form of plate-like particles. Mg is added to some alloys to strengthen by precipitation of Mg_2Si particles, but should be avoided in castings which are hardened by precipitation of Al_2Cu, as these elements tend to form a low melting point eutectic ($Al–Si–Al_5Mg_8Cu_2Si_6$), that takes place at temperatures below 500 °C. Strontium is added to modify the aspect of the Al–Si eutectic by promoting the formation of fibrous, coral-like, silicon branches, rather than coarse plates; titanium is added to refine grain size by promoting the nucleation of new grains in front of the solidifying front [7–11].

The onset of different solidification reactions can be determined with the aid of thermal analyses. The crudest interpretation of the phenomena taking place can be obtained by direct observation of the temperature–time curve, as most reactions are exothermic and result in the reduction in the cooling rate or, in some cases, can result in the increase in temperature due to recalescence [8,9,12,13]. These analyses can be conducted by inserting either one or more thermocouples in the mould containing the solidifying metal. Differences in temperature can be detected between different thermocouples, or the readings from one of these devices can be derived as a function of time to evaluate the time and temperature at which the reactions take place [2,8–11,14]. The aim of this work

* Corresponding author. Tel.: +52 81 83765159.
E-mail addresses: adrian.canales@cuprum.com.mx (A.A. Canales), jose.talamantes@nemak.com (J. Talamantes-Silva), david.gloria@nemak.com (D. Gloria), salvador.valtierra@owenscorning.com (S. Valtierra), rcolas@mail.uanl.mx (R. Colás).

0040-6031/$ – see front matter © 2010 Elsevier B.V. All rights reserved.
doi:10.1016/j.tca.2010.06.026

Table 1
Chemical composition of the experimental heats.

Heat	Si	Fe	Cu	Mn	Mg	Ti	Sr
5Si0.3Fe	5.303	0.286	3.148	0.446	0.296	0.110	130.9
5Si0.6Fe	4.980	0.601	3.356	0.439	0.277	0.071	100.2
5Si0.8Fe	5.070	0.805	3.261	0.467	0.289	0.071	113.6
7Si0.3Fe	6.950	0.325	3.150	0.452	0.292	0.166	127.4
7Si0.6Fe	6.813	0.592	3.166	0.450	0.280	0.155	119.7
7Si0.8Fe	6.776	0.764	3.133	0.450	0.319	0.163	136.7
9Si0.3Fe	9.064	0.307	3.320	0.441	0.301	0.149	132.4
9Si0.6Fe	9.068	0.609	3.192	0.462	0.299	0.143	143.0
9Si0.8Fe	8.726	0.811	3.132	0.450	0.286	0.130	115.1
11Si0.3Fe	10.816	0.321	3.425	0.436	0.270	0.143	142.5
11Si0.6Fe	10.807	0.588	3.499	0.436	0.278	0.139	111.0
11Si0.8Fe	10.736	0.782	3.461	0.437	0.259	0.141	69.3

Values in mass% for all elements except Sr that is given in ppm.

is to present the results obtained by the analysis of the derivation of the cooling curve recorded during the solidification of aluminium alloys prepared with different amounts of silicon and iron.

2. Experimental procedure

The experimental heats were prepared in a gas fired furnace to the nominal composition of 5, 7, 9 an 11% Si and 0.3%, 0.6% and 0.8% Fe. The amounts of Cu, Mn and Mg were kept within the 3.1–3.5%, 0.40–0.45% and 0.27–0.32% ranges, respectively. The melt was kept at 780 °C while degassing with nitrogen for 15 min; Ti and Sr were added before pouring the liquid into the moulds to promote grain refining and modification of the Al–Si eutectic aggregate, respectively. Table 1 shows the chemical composition of the experimental heats (the values are given in mass-% for all elements, except for Sr, which is given in ppm). The digits given in the table are those from the spark spectrometer used for the analyses, which was calibrated with special standards before each heat was analyzed. The low levels of strontium are due to the strong effect this element exerts on the morphology of the Al–Si eutectic aggregate.

The liquid metal was poured on graphite moulds of 50 mm in diameter by 50 mm in height that had a type K thermocouple to record the temperature at the centre of the mould, Fig. 1, which was connected to a computer-driven data logging system that feeds information into a portable computer. The moulds were immersed into the molten liquid for 60 s to equalize the temperature, the alloy was poured into the mould, and a graphite cover was placed on top to assure that the thermocouple remained in place during cooling. The experimental arrangement was placed on top of a ceramic blanket; a second blanket was placed on top of the mould to reduce the cooling rate.

The electromotive force from the thermocouples was recorded with a scanning rate of 5 Hz with the aid of a 16 bit analogue to digital conversion card; the accuracy in the conversion of electromotive force to temperature is ±0.25 °C; the confidence of the temperature readings given by the thermocouples is ±1.1 °C. The time derivative (dT/dt) was obtained by fitting a second-degree polynomial through an odd number of points from the cooling curves; dT/dt was evaluated at the mid-point of the odd data [2,10,11,14]. The aluminium specimens were sectioned and prepared for their metallographic observation following standard procedures.

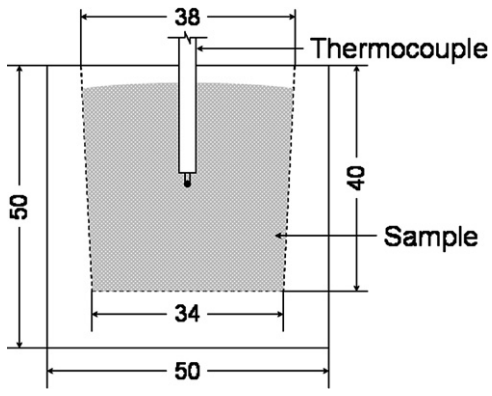

Fig. 1. Schematic diagram of the graphite moulds used in this work.

3. Results

Fig. 2 shows the cooling (temperature–time) curves obtained during the solidification of the four alloys with a nominal content of 0.6% Fe. A series of inflexions can be appreciated in all curves that correspond to different solidification reactions:

i. Growth of aluminium pre-eutectic dendrites.
ii. Growth of the Al–Si eutectic.
iii. Growth of a complex Al–Si–Cu–Mg eutectic.

These reactions affect the cooling rate as they are exothermic so the latent heat of transformation has to be released for solidification to proceed [12,13]. The onset of each of these reactions can be determined by plotting the time derivative as a function of time, or by plotting the temperature as a function of the derivative.

The analyses carried out for the case of the heats identified as 5Si0.3Fe and 11Si0.8Fe, see Table 1, are shown in Figs. 3 and 4 respectively. Three different curves are drawn in each figure; these are the cooling curve, T–t, the change of the time derivative as a

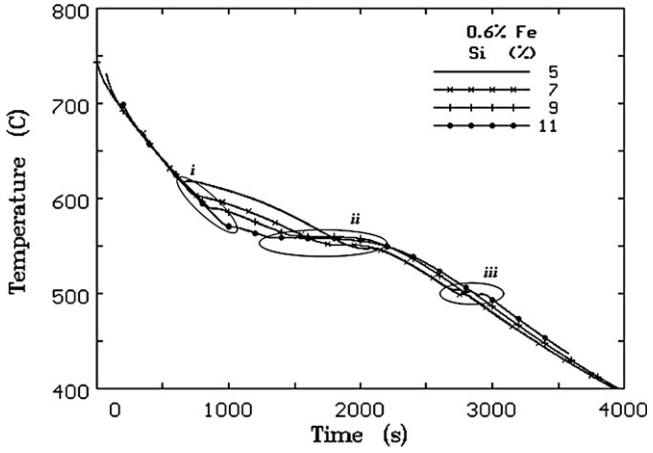

Fig. 2. Cooling curves for the alloys with a nominal composition of 0.6% Fe. The start of the test was displaced to make the initial slope to coincide; three solidification reactions are indicated.

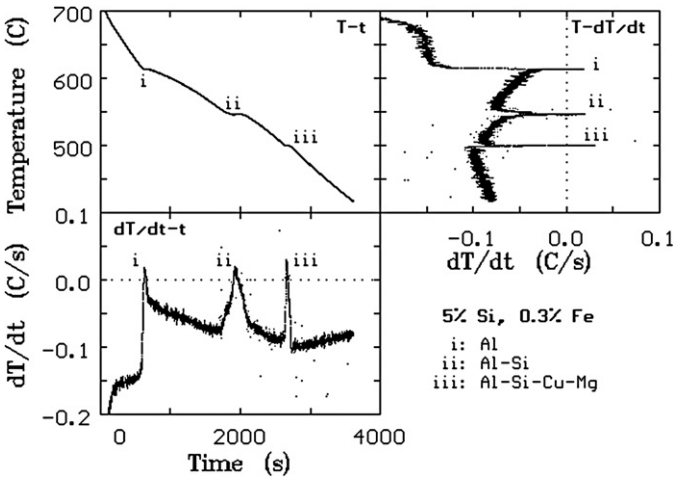

Fig. 3. Curves used for the analysis of an alloy with a nominal composition of 5% Si and 0.3% Fe; reactions *i*, *ii* and *iii* are indicated in each curve.

function of time, dT/dt–t, and the change of temperature as a function of the time derivative, T–dT/dt. It is worth noticing that the oscillations in the T–t curve transform into peaks in either dT/dt–t or T–dT/dt curve. The peaks and inflexions corresponding to the different reactions are identified in each of the curves shown in Figs. 3 and 4. Figs. 5 and 6 show the dT/dt–t curves for all the specimens; the corresponding T–dT/dt curves are shown in Figs. 7 and 8; the peaks corresponding to the various reactions can be identified from Figs. 3 and 4.

The microstructures from the samples with the nominal composition of 5% Si and 0.3% and 0.8% Fe are shown in Figs. 9 and 10, respectively; Figs. 11 and 12 show the microstructures corresponding to the samples cast with 11% Si and 0.3% and 0.8% Fe. The microstructure consists in pre-eutectic aluminium dendrites (that appear clear) surrounded by the Al–Si eutectic and other intermetallic phases and particles due to the elements present in the alloy.

4. Discussion

Data obtained during solidification were processed to determine the temperatures at which the various reactions proceed, as can be seen in Figs. 3 and 4. It is clear that the latent heat evolved during solidification change the oscillations on the T–t curve to peaks

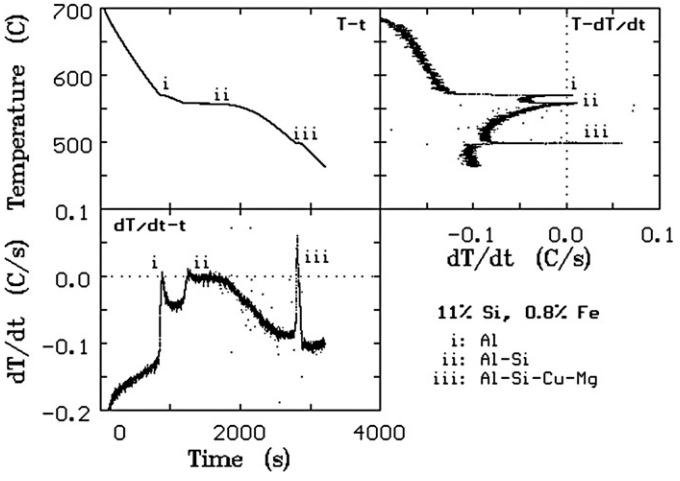

Fig. 4. Curves used for the analysis of an alloy with a nominal composition of 11% Si and 0.8% Fe; reactions *i*, *ii* and *iii* are indicated in each curve.

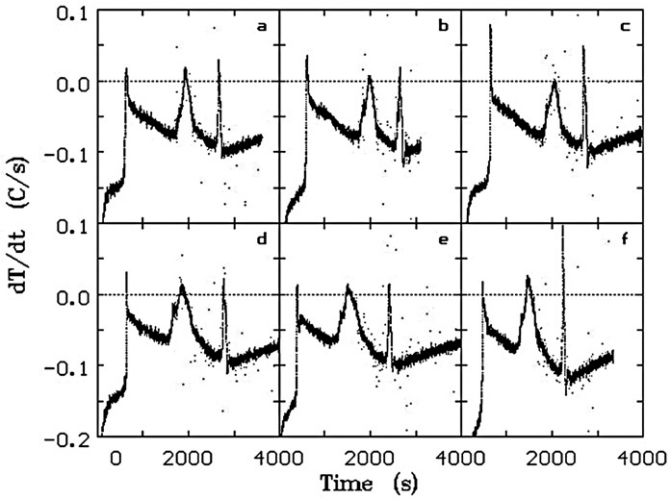

Fig. 5. dT/dt–t curves for heats 5Si0.3Fe (a), 5Si0.6Fe (b), 5Si0.8Fe (c), 7Si0.3Fe (d), 7Si0.6Fe (e) and 7Si0.8Fe (f).

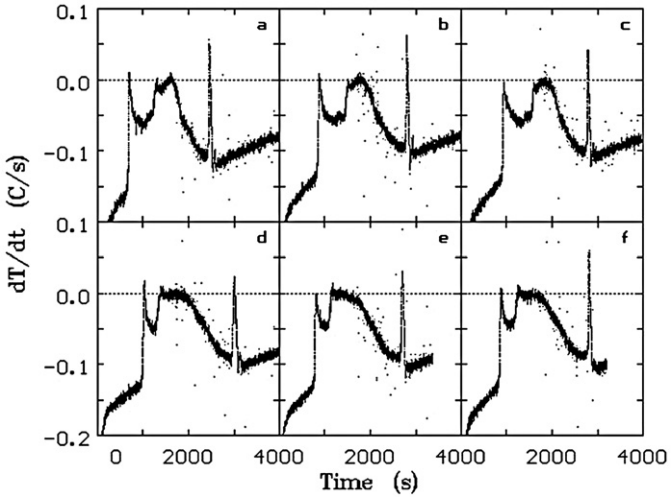

Fig. 6. dT/dt–t curves for heats 9Si0.3Fe (a), 9Si0.6Fe (b), 9Si0.8Fe (c), 11Si0.3Fe (d), 11Si0.6Fe (e) and 11Si0.8Fe (f).

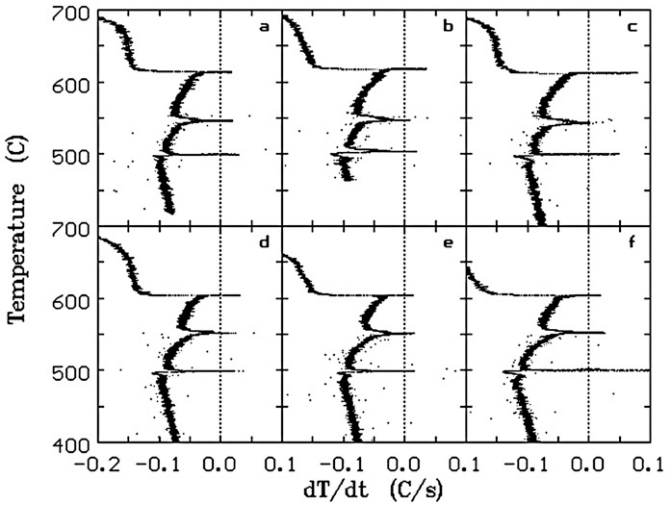

Fig. 7. T–dT/dt curves for heats 5Si0.3Fe (a), 5Si0.6Fe (b), 5Si0.8Fe (c), 7Si0.3Fe (d), 7Si0.6Fe (e) and 7Si0.8Fe (f).

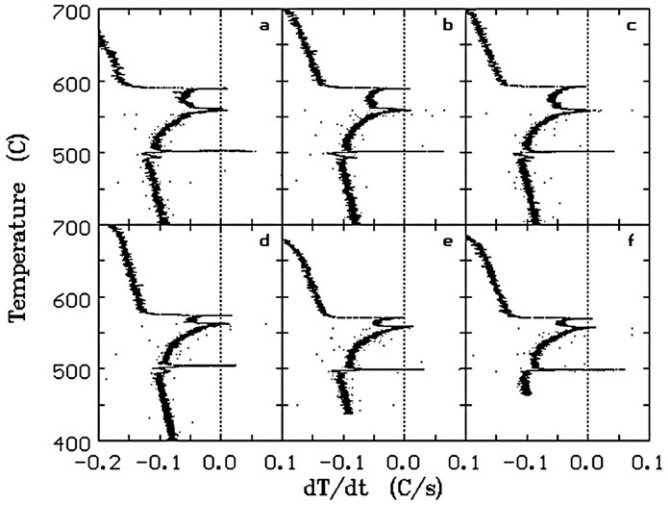

Fig. 8. *T–dT/dt* curves for heats 9Si0.3Fe (a), 9Si0.6Fe (b), 9Si0.8Fe (c), 11Si0.3Fe (d), 11Si0.6Fe (e) and 11Si0.8Fe (f).

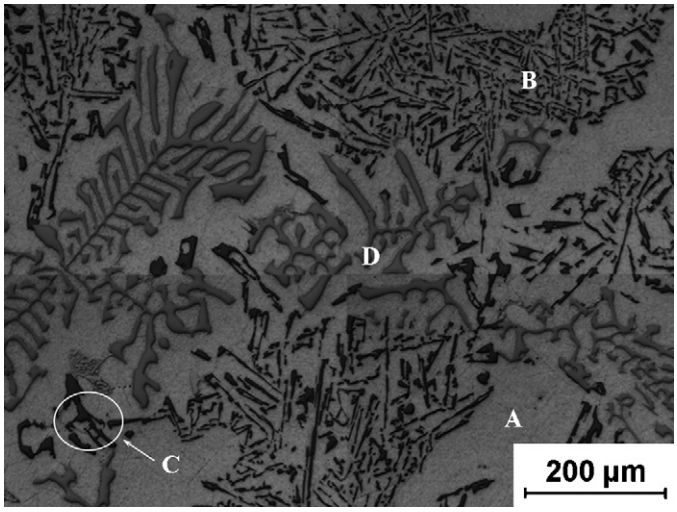

Fig. 11. Microstructure of the specimen with a nominal composition of 11% Si and 0.3% Fe; components as in Fig. 9.

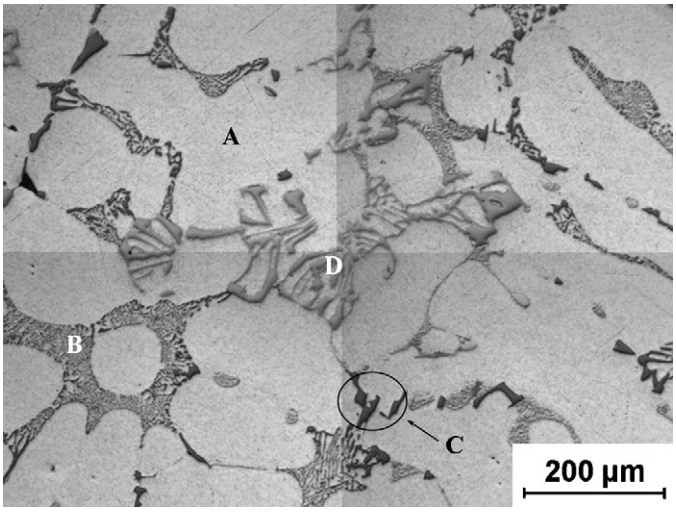

Fig. 9. Microstructure of the specimen with a nominal composition of 5% Si and 0.3% Fe; the components are Al dendrites (A), Si–Al eutectic (B) Al–Si–Cu–Mg eutectic (C) and Chinese typescript inclusions (D).

in either the *dT/dt–t* or *T–dT/dt* curve, due to the drastic change in cooling rate, but the scatter generated during the numerical derivation does not allow for a clear interpretation of the curves, so it was required to present them in Figs. 5–8. The curves shown in Figs. 5 and 6 correspond to the *dT/dt–t* curves in which the reactions *i*, *ii* and *iii* are shown occur from left to right. Care was taken during the experimentation to maintain a constant cooling rate, see Fig. 2, to simplify the analyses. The curves in Figs. 5 and 6 shows that the time between reactions *i* and *ii* is reduced as the amount of silicon added to the melt increases. The shape of the peak due to the formation of the Al-Si eutectic (reaction *ii*) also changes with the amount of silicon, as the peaks tend to broaden and reduce their height, which translates into a shorter but greater recalescence in the cooling (*T–t*) curves of the material with less silicon, see Fig. 2. The reaction that shows the highest recalescence is the one corresponding to the complex Al–Si–Cu–Mg eutectic (*iii*).

Figs. 7 and 8 show the *T–dT/dt* curves; in this case reactions *i*, *ii* and *iii* are shown to occur from top to bottom as the curves are plotted following the scheme of Figs. 3 and 4. The sharp peaks indicate that the reactions occur at fairly constant temperature, although small changes in temperature occur due to recalescence. These curves show that the difference in temperature between reactions

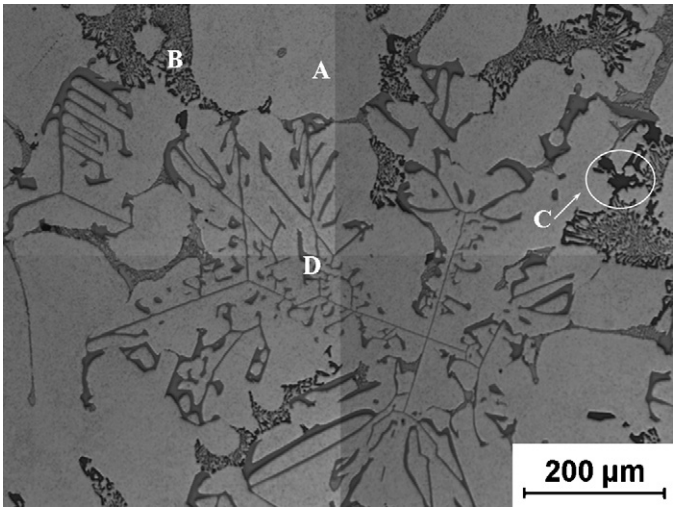

Fig. 10. Microstructure of the specimen with a nominal composition of 5% Si and 0.8% Fe; components as in Fig. 9.

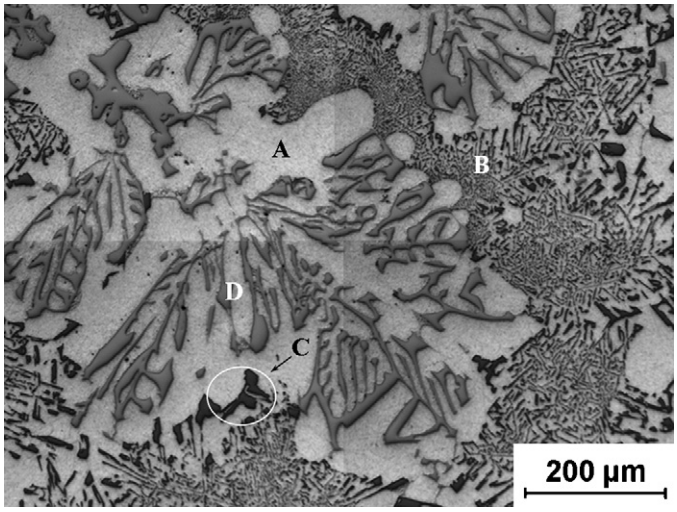

Fig. 12. Microstructure of the specimen with a nominal composition of 11% Si and 0.8% Fe; components as in Fig. 9.

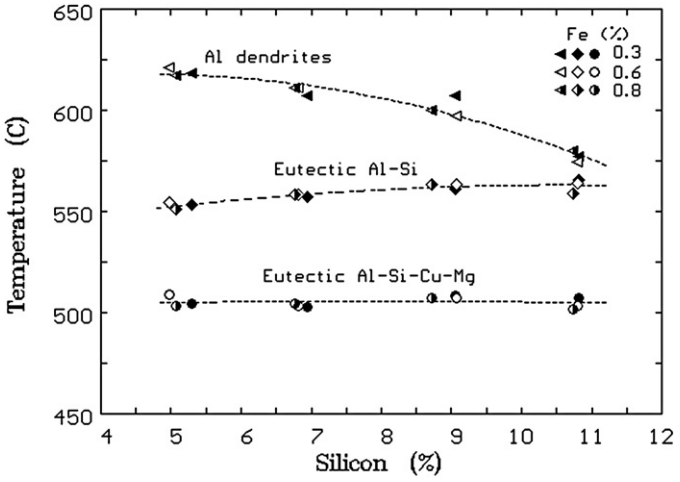

Fig. 13. Dependence of the onset for different solidification reactions as a function of silicon content.

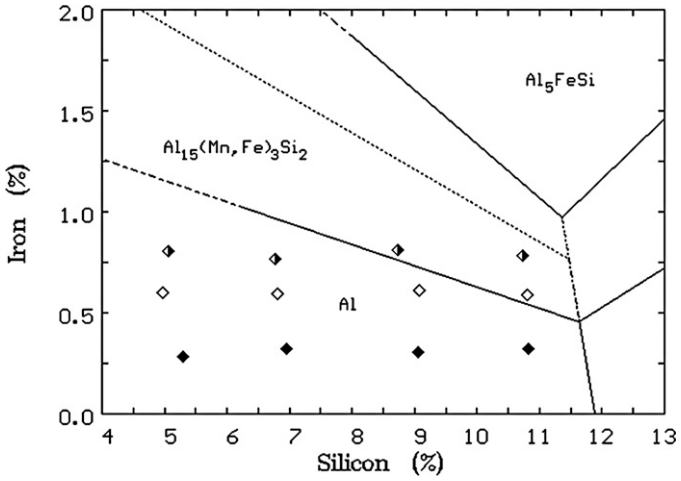

Fig. 15. Al-rich corner of the Al–Si–Fe diagram with 0.4% Mn [16] showing the occurrence of different phases.

i and *ii* is reduced with the increase of silicon, and that the temperature for the onset of reaction *iii* is independent of either the increase of iron or silicon. These findings are summarized in Fig. 13 in which the temperature dependence for the onset of the various reactions is plotted as a function of silicon content, and, as it can be seen, silicon exerts a great influence on the onset for reactions *i* and *ii*, but not for reaction *iii*. No effect of iron on the temperature for the onset of reaction *i* was found, although it has been reported that iron affects this reaction when no refining elements are added [11]. The reduction in temperature for the onset or reaction *i* follows the reduction in the temperature for liquidus in equilibrium for the Al–Si and Al–Cu–Si systems [15], Fig. 14.

The micrographs shown in Figs. 9–12 are typical of hypoeutectic aluminium–silicon alloys; the aspect of the Al–Si eutectic appears well modified in Figs. 9 and 10 due to the higher amount of Sr added to these particular castings. It is clear that the amount of the eutectic increases with the increment in silicon. The iron intermetallics observed in all cases exhibit the Chinese type script shape that corresponds to the α-type or $Al_{15}(Mn,Fe)_3Si_2$ as manganese promotes the formation of this type over the more deleterious β-type (Al_5FeSi) [8,16]. The blocky particles that appear dark in the microstructures correspond to copper-rich particles that are part of the complex Al–Si–Cu–Mg eutectic. The conditions for the occurrence of the different types of iron intermetallics can be deduced from the aluminium rich corner of the Fe–Si–Al diagram, which for the case of 0.4% Mn [16] is shown in Fig. 15 together with the chemical composition of the experimental heats. It can be deduced from this figure that the only intermetallics that can be formed will be of the α-type (Chinese script), as is appreciated in the micrographs of Figs. 9–12.

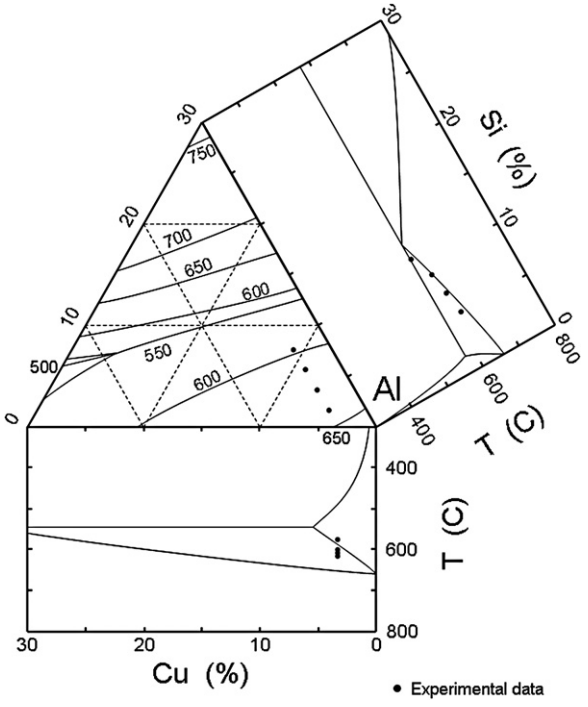

Fig. 14. Data points for the onset of reaction *i* as a function of silicon and copper contain; phase diagrams from Ref. [15].

The results of the studies presented in this work were used to improve the processing conditions in the cast shop, as some of the liquid alloys to be cast into automotive parts are prepared with varying amounts of primary ingots and scrap, so the limits of trace elements, among them iron being considered most critical, can be defined by this type of work.

5. Conclusions

The reactions that take place during the solidification of aluminium castings alloys were detected by the numerical derivation of the cooling curve recorded with an inserted thermocouple. The thermal analyses show that the temperatures for the onset of the formation of pre-eutectic aluminium dendrites and that for the formation of the aluminium-silicon eutectic depend on the amount of silicon added to the experimental heat. No effect of iron on the onset for the formation of pre-eutectic dendrites was found. The temperature at which the complex Al–Si–Cu–Mg eutectic is formed is unaffected by either silicon or iron.

The microstructures in the experimental heats are characteristic of hypoeutectic Al–Si alloys, in which the amount of the eutectic aggregate increases with the increase of silicon. The iron rich intermetallics were of the α-type due to the modifying effect of manganese present in the experimental heat.

Acknowledgements

The authors acknowledge the support provided by the National Council for Science and Technology (CONACYT), Mexico, and the Program for the Support for Science and Technology Research (PAICYT), from UANL.

References

[1] J. Campbell, Castings, 2nd ed., Butterworth-Heinemann, Oxford, 2003.
[2] R. Colás, E. Velasco, S. Valtierra, Castings, Handbook of aluminum, in: G.E. Totten, D.S. MacKenzie (Eds.), Physical Metallurgy and Processes, 1, M. Dekker, New York, 2003, pp. 591–641.
[3] J.B. Heywood, Internal Combustion Engine Fundamentals, McGraw-Hill, New York, 1989.
[4] P.M. Norris, M.C. Hastings, W.J. Wepfer, J. Exp. Heat Trans. 7 (1994) 43–51.
[5] J.B. Heywood, Internal Combustion Engine Fundamentals, McGraw-Hill Int. Ed., New York, 1989.
[6] R.B. Gundlach, B. Ross, A. Hetke, S. Valtierra, J.F. Mojica, Trans. AFS 104 (1994) 205–211.
[7] I.J. Polmear, Light Alloys, Metallurgy of the Light Metals, Arnold, London, 1980.
[8] L. Bäckerud, G. Chai, J. Tamminen, Solidification Characteristics of Aluminum Alloys Foundry Alloys, vol. 2, AFS/Skanaluminium, Des Plains, 1990.
[9] L. Arnbert, L. Bäckerud, G. Chai, Solidification Characteristics of Aluminum Alloys Dendritic Coherency, vol. 3, AFS, Des Plains, 1996.
[10] R. Colás, A. Rodríguez, J. Talamantes, S. Valtierra, Solidification analysis of aluminium engine block, Int. J. Cast Met. Res. 17 (2004) 332–338.
[11] R. Torres, J. Esparza, E. Velasco, S. García-Luna, R. Colás, Int. J. Microstruct. Mat. Prop. 1 (2006) 129–138.
[12] R.D. Shull, in: R.D. Shull, A. Joshi (Eds.), Thermal Analysis in Metallurgy, TMS, Warrendale, 1992, p. 75.
[13] H. Biloni, W.J. Boettinger, Solidification, in: R.W. Cahn, P. Haasen (Eds.), Physical Metallurgy, 4th ed., North Holland, Amsterdam, 1996, pp. 669–842.
[14] E. Velasco, J. Talamantes, S. Cano, S. Valtierra, J.F. Mojica, R. Colás, Metall. Mater. Trans. B 30B (1999) 773–778.
[15] ASM Handbook Alloy Phase Diagrams, vol. 3, ASM International, Materials Park, 1992.
[16] W. Khalifa, A.M. Samuel, F.H. Samuel, H.W. Doty, S. Valtierra, Int. J. Cast Met. Res. 19 (2006) 156–166.